Near-Capacity UWB Impulse Radio Using EXIT Chart Aided Self-Concatenated Codes

R. A. Riaz[1,2], M. F. U. Butt[1,2], S. X. Ng[1], S. Chen[1] and L. Hanzo[1]
[1]School of ECS, University of Southampton, SO17 1BJ, United Kingdom.
Email: {rar06r, mfub06r, sxn, sqc, lh}@ecs.soton.ac.uk, http://www-mobile.ecs.soton.ac.uk
[2]Dept of EE, COMSATS Institute of Information Technology, Islamabad, 44000, Pakistan, http://ciit.edu.pk

***Abstract*— A near-capacity Time Hopping (TH) Pulse Position Modulation (PPM) based UltraWideBand (UWB) Impulse Radio (IR) system is proposed, which invokes iteratively detected Self-Concatenated Convolutional Codes (SeCCC) and employs powerful design technique of Extrinsic Information Transfer (EXIT) charts. Orthogonal Prolate Spheroidal Wave Function (OPSWF) based signalling pulse shapes are used for the sake of minimizing the Multi-User Interference (MUI) and Inter-Symbol Interference (ISI). Recursive Systematic Convolutional (RSC) codes are employed as constituent codes combined with an interleaver for randomising the extrinsic information exchange between the constituent codes. Furthermore, a puncturer assists us in increasing the achievable bandwidth efficiency. Iterative decoding is invoked for exchanging extrinsic information between the hypothetical decoder components at the receiver end. The convergence behaviour of the decoder is analysed with the aid of bit-based EXIT charts. Finally, we propose a novel TH-PPM-UWB-IR-SeCCC system configuration, which is capable of operating within about 0.9 dB of the information-theoretic limits.**

I. Introduction

According to the Federal Communications Commission (FCC), UltraWideBand (UWB) systems generate a signal that occupies at least 500MHz of bandwidth in the 7.5GHz spectral band between 3.1GHz and 10.6GHz. This definition also includes some rather strict limits on both the radiated power and the power spectral density [1]. Hence the properties of UWB systems are fundamentally different from those of classic cellular communications. Instead of using a carrier frequency, as in GSM networks, UWB signals may be generated based on sending and receiving very high-bandwidth carrierless radio impulses using extremely accurate timing [2].

One of the most important UWB modulation technique is constituted by Time Hopping (TH), which is based on the classic Impulse Radio (IR) concept developed by Scholtz and Win [2] although multi-stage frequency hopping was also proposed as a beneficial design alternative [3]. The concept of TH Pulse Position Modulation (PPM) aided UWB IR systems is that trains of time-shifted PPM pulses are used to transmit baseband or carrierless UWB signals. One of the attractive features of TH-PPM-UWB systems is their strong multipath interference mitigating capability.

The generic philosophy of concatenated coding schemes was proposed by Forney in [4]. Turbo codes constitute a class of error correction codes (ECC) based on parallel concatenated convolutional codes (PCCC) of two or more constituent codes, which were developed by Berrou $et.\ al.$ [5]. They are high-performance codes capable of operating near the Shannon limit [6]. Serially concatenated convolutional codes (SCCC) [7] have also been shown to yield a performance comparable, and in some cases superior, to classic turbo codes. The class of iteratively-decoded Self-Concatenated Convolutional Codes (SeCCC) proposed by Benedetto *et al.* [8] and Loeliger [9] constitute another attractive family of iterative detection aided schemes.

The concept of Extrinsic Information Transfer (EXIT) charts was proposed by ten Brink [10] as a tool designed for analysing the convergence behaviour of iteratively decoded systems. EXIT charts constitute a semi-analytical tool that can also be used to predict the SNR value, where an infinitesimally low Bit Error Ratio (BER) can be achieved, while dispensing with time-consuming bit-by-bit decoding employing a high number of decoding iterations.

TH-PPM-UWB-IR systems are popular owing to their low-complexity implementation, since they do not invoke carrier modulation. However, it is a grave challenge to design an UWB system having a high bandwidth, while requiring relatively low-complexity signal processing algorithms for mitigating the Inter-symbol Interference (ISI) and Multiuser Interference (MUI). Hence, conventional TH-PPM-UWB-IR detection schemes [11] typically fail to perform near the attainable capacity. Hence our goal is to design near-capacity UWB systems having a moderate complexity. Therefore we invoke a low-complexity SeCCC scheme employing a single encoder and a single decoder, since the amalgam of TH-PPM-UWB-IR and SeCCC constitutes an attractive near-capacity design alternative.

Hence the novel contribution of this treatise is that we design a near-capacity iteratively decoded TH-PPM-UWB-IR-SeCCC system using EXIT charts. More explicitly, the powerful tool of EXIT charts is used to appropriately select the coding rates of the SeCCCs in order to shape the inverted EXIT curve of the TH-PPM-UWB-IR-SeCCC system and hence to match it with that of the inner decoder for the sake of achieving an infinitesimally low Bit Error Ratio (BER) at near-capacity SNR values. The proposed design is capable of low Signal-to-Noise Ratio (SNR) operation in Nakagami-m fading channels. The associated iterative decoding convergence behaviour is characterized by EXIT Charts. The proposed TH-PPM-UWB-IR-SeCCC design becomes capable of performing within about 0.9 dB of the Nakagami-m fading channel's capacity.

The organisation of the paper is as follows. We commence by elaborating on our system model in Section II, while we discuss the UWB transceiver in Section III. Section IV details our Exit-Chart based methodology used for finding the optimal code parameters. Our results are discussed in Section V, while our conclusions are offered in Section VI.

The financial support of the EPSRC UK, EU Optimix project as well as of the COMSATS Institute of Information Technology is gratefully acknowledged.

978-1-4244-2515-0/09/$25.00 ©2009 IEEE

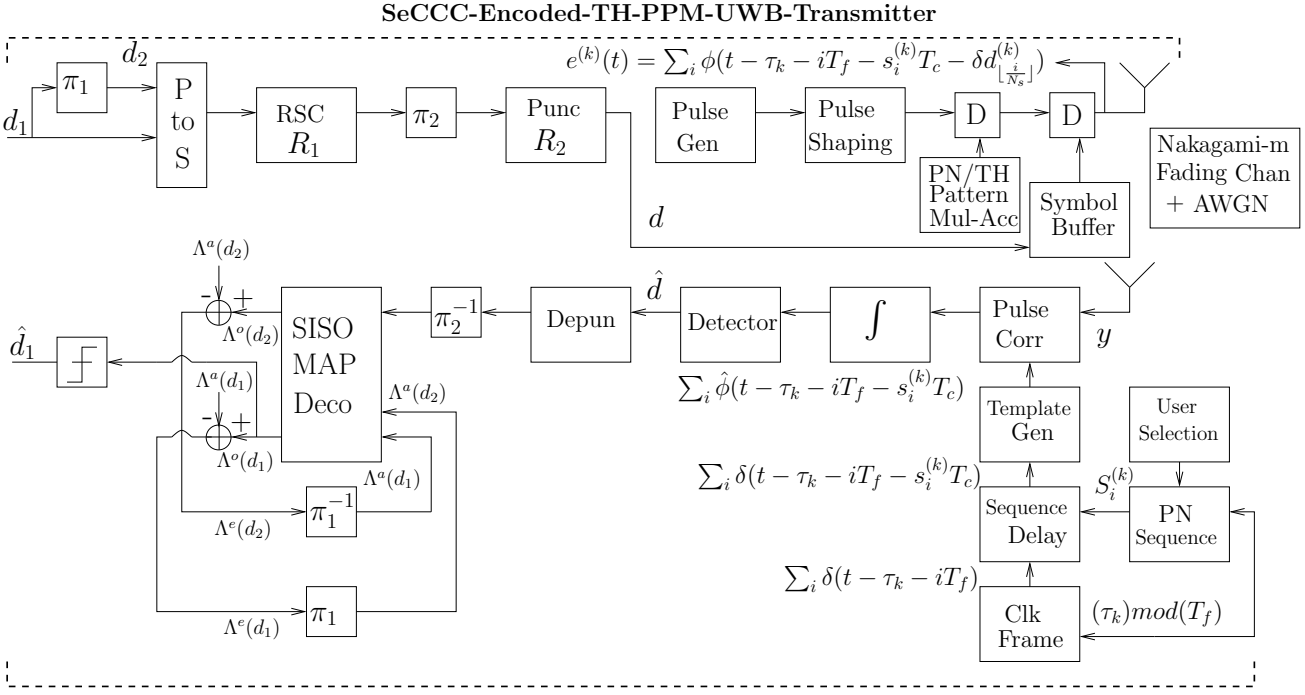

Fig. 1. TH-PPM-UWB-IR-SeCCC System

II. System Model

Fig. 1 shows the baseband model of the iteratively detected TH-PPM-UWB-IR-SeCCC system. We have used Orthogonal Prolate Spheroidal Wave Function (OPSWF) signalling pulses and PPM for transmission over uncorrelated Nakagami-m fading channels. A rate $R = \frac{1}{2}$ SeCCC scheme is considered in order to highlight the various system concepts in this paper.

As shown in Fig. 1, the input bit sequence $\{d_1\}$ of the self-concatenated encoder is interleaved for yielding the bit sequence $\{d_2\}$. The resultant bit sequences are parallel-to-serial converted and then fed to the Recursive Systematic Convolutional (RSC) encoder using the generator polynomials of $(13, 15, 17)$ expressed in octal format and having a rate of $R_1 = \frac{1}{3}$ as well as a memory of $\varphi = 3$. Hence, for every bit input to the SeCCC encoder there are six output bits generated by the RSC encoder. At the output of the encoder there is an interleaver and a rate-$R_2 = \frac{1}{3}$ puncturer, which punctures (i.e. obliterates) two bits out of three encoded bits. Hence, the overall code rate, R can be derived based on [12] as:

$$R = \frac{R_1}{2 \times R_2} = \frac{1}{2}\left(\frac{1}{3\left(\frac{1}{3}\right)}\right) = \frac{1}{2}. \tag{1}$$

Therefore, at the output of the puncturer the number of encoded bits reduces from six to two, namely to $(b_0 b_1)$. Again, puncturing is used in order to increase the achievable bandwidth efficiency η. It can be observed that different codes can be designed by changing R_1 and R_2 in order to achieve the best possible performance. The bits d seen in Fig. 1 are then sent to the bit-to-symbol conversion buffer. The resultant symbols are then pulse position modulated, while obeying the OPSWF pulse shapes in order to minimize the effects of ISI and MUI. Finally, the TH-PPM-UWB-IR-SeCCC encoded transmitted signal is formed by invoking a Pesudo-Noise (PN) generator for creating the required TH patterns obeying the corresponding PPM signalling delays, as shown in Fig. 1. The resultant transmitted signal is characterized in Section III.

After transmission over a non-dispersive Nakagami-m fading channel contaminated by Additive White Gaussian Noise (AWGN) having a variance of $\frac{N_0}{2}$ per dimension, the received signal y is fed into a pulse-position correlation detector, as shown in Fig. 1. The closed-form matrix description of the receiver is detailed in Section III. After the TH-UWB-PPM-IR detector the signal $\hat{d}$ is then used by a soft demapper for calculating the conditional probability density function (PDF) of receiving y, when $e^{\{(k),(m)\}}$ was transmitted, where k is the number of users and the set $m \in \{0, 1, 2, 3\}$ represents the legitimate quarternary modulated symbols. Then, these PDFs are passed to a soft depuncturer, which converts the PDFs to bit-based Log-Likelihood Ratios (LLRs) denoted by Λ in Fig.1 and inserts zero LLRs at the punctured bit positions. These LLRs are then deinterleaved and fed to the Soft-Input Soft-Output (SISO) *Maximum A Posteriori Probability* (MAP) decoder [13]. The decoder is a self-concatenated decoder. It first calculates the extrinsic LLRs of the information bits, namely $\Lambda^e(d_1)$ and $\Lambda^e(d_2)$, which are appropriately interleaved to generate the *a priori* LLRs of the information bits, namely $\Lambda^a(d_1)$ and $\Lambda^a(d_2)$, as shown in Fig. 1. Self-concatenated decoding proceeds, until the affordable number of iterations is reached.

III. UWB Transceiver

A. Transmitted Signal

The TH-PPM-UWB signal transmitted by the k^{th} user is given by [14]:

$$e^{(k)}(t) = \sum_i \phi(t - iT_f - s_i^{(k)} T_c - \delta d^{(k)}_{\lfloor \frac{i}{N_s} \rfloor}), \tag{2}$$

where $\phi(t)$ is the transmitted monocycle waveform, T_f is the frame time or pulse repetition time, which is hundred to a thousand times the monocycle width, $s_i^{(k)}$ is the unique user-specific TH code of each user having a period of N_p, T_c is the discrete time shift engendered by the TH code of each user

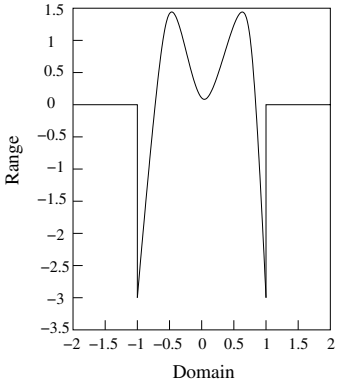

Fig. 2. Fourth-order OPSWF.

and δ represents the time shift of the monocycle corresponding to the modulating symbol. Furthermore, $d_i^{(k)}$ in eq (2) is the data sequence of user k, and in our oversampled modulation scheme N_s monocycles are transmitted per modulating symbol, where the modulating data symbol changes only every N_s hops i.e. there are N_s hops per modulating symbol, where we assume that a new data symbol begins at the signalling pulse index $i = 0$ and the index of the signalling pulse i obeys $\lfloor \frac{i}{N_s} \rfloor$. Here the notation $\lfloor x \rfloor$ denotes the floor function.

B. Pulse Shape

The OPSWFs yield orthogonal pulses that have a constant pulse width and bandwidth, regardless of the pulse order, which is in contrast to the majority of other orthogonal pulse classes. These OPSWFs are generated by solving [15]

$$\int_{\frac{-T}{2}}^{\frac{T}{2}} \phi_n(y) \frac{sin\Omega(t-y)}{\pi(t-y)} dy = \lambda_n \phi_n(t), \tag{3}$$

or, alternatively, by solving the differential equation

$$\frac{d}{dt}(1-t^2)\frac{d\phi_n(t)}{dt} + (\Xi_n - v^2 t^2)\phi_n(t) = 0, \tag{4}$$

where $\phi_n(t)$ are PSWFs of order n and Ξ_n represents the eigenvalues of $\phi_n(t)$. The constant v is given by

$$v = \frac{\Omega T}{2}, \tag{5}$$

where Ω is the bandwidth and T is the signalling pulse duration. In eq (3), λ_n characterizes the concentration of energy in the interval $[\frac{-T}{2}, \frac{T}{2}]$. More explicit details regarding OPSWFs can be found in [16]. In this contribution, we have used fourth-order OPSWFs, schematically shown in Fig. 2.

C. Channel Model

The CIR model ratified by the IEEE 802.15.3 standard and considered here can be expressed as [17]

$$h(t) = \sum_{r=1}^{R} h_r e^{j\varphi_r} \delta(t - rT_\varphi), \tag{6}$$

where R represents the number of resolvable paths, while h_r and φ_r are the gain and phase of the rth resolvable multipath component. Furthermore, rT_φ represents the corresponding delay of the rth multipath component.

As shown in [18], [19], the CIR taps of the UWB channel follow the Nakagami-m distribution, which has been validated by using the Kolmogorov-Smirnov testing at a significance level of 1%. More explicitly, the fading gains h_r obey an independent Nakagami-m distribution with a probability density function (PDF) of the envelop c given by [20]

$$P_{h_r}(c) = \frac{2m_r^{m_r} r^{2m_r-1}}{\Gamma(m_r)\Omega_r^{m_r}} e^{\frac{-m_r c^2}{\Omega_r}}, \qquad c > 0 \tag{7}$$

where m_r is the Nakagami fading parameter defined as:

$$m_r = \frac{E^2\left[c^2\right]}{var(c^2)}, \tag{8}$$

while the parameter Ω_r is $E\left[c^2\right]$. Furthermore, the moments of the random variable c are given by:

$$E\left[c^v\right] = \frac{\Gamma\left(m_r + \frac{v}{2}\right)}{\Gamma(m_r)} \left(\frac{\Omega}{m_r}\right)^{\frac{v}{2}}. \tag{9}$$

Finally, $\Gamma(\cdot)$ is the gamma function defined as

$$\Gamma(m_r) = \int_0^\infty x^{m_r-1} e^{(-x)} dx. \tag{10}$$

We assume in our analysis that the phase rotation of the fading channel is uniformly distributed in $[0, 2\pi]$. Let us now consider the receiver structure.

D. Receiver Model

The discretised composite received signal can be expressed as

$$\mathbf{y} = \mathbf{A}\mathbf{d} + n, \tag{11}$$

where A is the overall system matrix, d is the symbol sequence after SeCCC encoding, while n represents the AWGN sequence, which has a covariance matrix of $R_n = E[nn^H]$. The pre-detection signal processing steps are schematically detailed in Fig. 1. The whole process can be represented in a closed matrix form as [21]

$$\hat{\mathbf{d}} = \underbrace{diag(\mathbf{A}^H R_n^{-1}\mathbf{A})\mathbf{d}}_{symbols} + \underbrace{\overline{diag}(\mathbf{A}^H R_n^{-1}\mathbf{A})\mathbf{d}}_{ISI,MAI} + \underbrace{\mathbf{A}^H R_n^{-1} n}_{noise}. \tag{12}$$

In the next section we detail our design procedure devised for achieving a near-capacity performance by the TH-PPM-UWB-IR system with the aid of EXIT charts.

IV. EXIT Charts Design Methodology

EXIT charts constitute a powerful tool designed for analysing the convergence behaviour of concatenated codes without time-consuming bit-by-bit Monte-Carlo simulation of the actual system. They analyse the input/output mutual information characteristics of a SISO decoder by modelling the *a priori* LLRs and computing the mutual information between the extrinsic LLRs and the corresponding bit-decisions. However, the employment of EXIT charts assumes having a sufficiently high interleaver length, so that the extrinsic LLRs can be rendered independent Gaussian distributed. The SNR value, where the turbo-cliff [5] in the BER curve of a concatenated code appears can be successfully predicted with the aid of EXIT charts.

The EXIT charts of self-concatenated codes are typically similar to those of the parallel concatenated TTCM schemes [22, 23], where an open EXIT tunnel exists if the

EXIT curve does not intersect the straight line connecting the point ($I_A = 0$, $I_E = 0$) to the point ($I_A = 1$, $I_E = 1$) in the EXIT chart. The various coding schemes considered in this paper are characterised in Table I. They are identified by the code rate (R_1), puncturing rate (R_2), overall code rate (R), code memory φ and bandwidth efficiency expressed in bit/s/Hz, as η . The $\frac{E_b}{N_o}$ decoding convergence threshold, beyond which the EXIT tunnel becomes "just" open is denoted by T_h, although this does not necessarily imply that the (I_A, I_E)=(1,1) point of 'perfect convergence' can be reached, because some of the decoding trajectories are curtailed owing to the limited interleaver length used. This is why the slightly different term, tunnel T_l was introduced, which specifies the $\frac{E_b}{N_o}$ value, where there is a more widely open EXIT tunnel leading to the (1,1) point and where decoding convergence to an infinitesimally low BER value can always be achieved, provided that the interleaver length is large and the number of decoding iterations is sufficiently high [10]. Furthermore, the channel capacity limit ω is also expressed in dBs [24], as tabulated in Table I. For R_1=1/2 and $\varphi = 2$, the octally represented generator polynomial of $G = (7, 5)$ is used, whereas for $\varphi = 3$, $G = (13, 15)$ is employed. For R_1=1/3 and $\varphi = 3$, $G = (13, 15, 17)$ is used.

TH-PPM-UWB-IR-SeCCC System	φ	η (bit/s /Hz)	Nakagami-m Channel E_b/N_0 (dB)		
			T_h	T_l	ω
R_1=1/2,R_2=3/4, R=1/3	2	0.67	2.5	2.7	1
	3	0.67	1.8	1.9	1
R_1=1/2,R_2=1/2, R=1/2	2	1	4.5	4.6	1.83
	3	1	3.5	3.6	1.83
R_1=1/2,R_2=1/3, R=3/4	2	1.5	13	13.6	6
	3	1.5	9.2	9.4	6
R_1=1/3,R_2=2/3, R=1/4	3	0.5	1.2	1.3	-0.2
R_1=1/3,R_2=1/3, R=1/2	3	1	3.5	3.6	1.83
R_1=1/3,R_2=1/4, R=2/3	3	1.33	6.4	6.6	3

TABLE I

VARIOUS TH-PPM-UWB-IR-SECCC SYSTEM'S DECODING CONVERGENCE THRESHOLDS AND EXIT TUNNELS. φ:MEMORY OF SECCC, η:BANDWIDTH EFFICIENCY, ω:CHANNEL CAPACITY LIMIT AND T_h,T_l:CONVERGENCE THRESHOLD

The EXIT charts recorded for the TH-PPM-UWB-IR-SeCCC system of Table I are shown in Fig. 3. The two EXIT curves represent the two hypothetical decoder components of the SeCCC scheme, while the stair-case-shaped trajectory "snap-shots" correspond to iterating between them. Since these are identical components, we only have to compute the EXIT curve of one component and the other is its mirror image with respect to the diagonal line. The EXIT curves of the hypothetical decoder components are plotted within the same EXIT chart together with their corresponding decoding trajectory for the sake of visualizing the transfer of extrinsic information between the decoders. The EXIT curves of the proposed scheme exactly match the decoding trajectories computed from the bit-by-bit simulations.

The EXIT curves and the two distinct decoding trajectories were recorded for the best-performing TH-PPM-UWB-IR-SeCCC system operating closest to the Nakagami-m channel's capacity, which are given in Fig. 3 for a specific bit-by-bit simulation. Similar decoding trajectory snapshots were found for all our simulations. These were recorded by using 10^3 transmission frames, each consisting of 24×10^3 information bits for calculating the EXIT curve, and 10^3 frames each consisting of 120×10^3 information bits for calculating the decoding trajectories respectively.

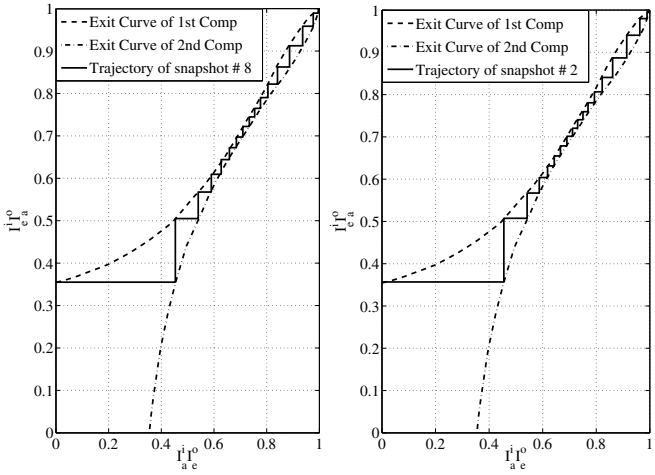

Fig. 3. EXIT chart and decoding trajectories for R_1=1/2 and R_2=3/4, TH-PPM-UWB-IR-SeCCC, $\varphi = 3$, $\eta = 0.67$ bit/s/Hz at $\frac{E_b}{N_o} = 1.9$ dB, for transmission over a Nakagami-m fading channel.

In Fig. 3, the scheme using $R_1 = 1/2$, $R_2 = 3/4$, $\varphi = 3$ succeeds in creating an open EXIT tunnel at $\frac{E_b}{N_o}$=1.9 dB, when communicating over an uncorrelated Nakagami-m fading channel. For this scheme the threshold T_h is reached at 1.8 dB according to Table I, which is 0.8 dB away from capacity.

The employment of the interleaver, π_1 seen in Fig. 1 and used in all of the schemes considered in Table I renders the information bits more-or-less uncorrelated. This is a necessary condition for the employment of EXIT charts, because they require the LLRs of the information bits to be Gaussian distributed. The interleaver used after the RSC encoder of Fig. 1, namely π_2, randomises the coded bits before the puncturer.

V. RESULTS AND DISCUSSIONS

The EXIT charts discussed in Section IV were used to find the best TH-PPM-UWB-IR-SeCCC system parameters for $\varphi = \{2, 3\}$, when communicating over uncorrelated Nakagami-m fading channels.

The convergence threshold predicted by the EXIT chart analysis detailed in Section IV closely matches the actual convergence threshold observed in the BER curve given by the specific $\frac{E_b}{N_o}$ value, where there is a sudden drop of the BER after a certain number of decoding iterations, as shown in Fig. 4. Hence it becomes possible to attain an infinitesimally low BER beyond the convergence threshold T_h, provided that both the block length and the number of decoding iterations are sufficiently high.

The BER versus $\frac{E_b}{N_o}$ performance curves of the various TH-PPM-UWB-IR-SeCCC systems recorded from our bit-by-bit simulations are shown in Fig. 4. As mentioned, we considered an information block length of 120×10^3 bits per frame, transmitted 10^3 frames and the number of decoding iterations (I) varied from 50 to 80. Fig. 4 shows the $\frac{E_b}{N_o}$ difference

between the capacity and the convergence threshold T_h for the best TH-PPM-UWB-IR-SeCCC system at a given code memory φ.

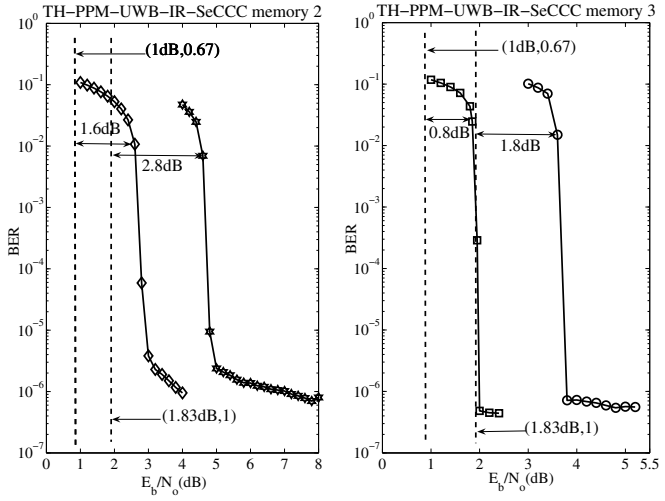

Fig. 4. The BER versus E_b/N_0 performance of various TH-PPM-UWB-IR-SeCCC system, R_1 = 1/2, R_2=3/4 and $I = 80$ decoding iterations for $\varphi = 2$ and $I = 50$ decoding iterations for $\varphi = 3$, operating over uncorrelated Nakagami-m fading channel.

It can be observed from Fig. 4 that the system using $R_1 = 1/2$, $R_2 = 3/4$ and $\varphi = 2$ is capable of operating within 1.6 dB and 2.8 dB of the Nakagami-m fading channel's capacity, respectively. As observed from Table I, in the case of a lower puncturing rate yielding a code rate of $R_2 = 1/3$ and $R_1 = 1/2$, the memory $\varphi = 3$ code performs better compared to the $\varphi = 2$ code.

As we can see by studying Table I and Fig. 4, the actual BER convergence threshold is exactly the same as the convergence threshold predicted by the EXIT charts. Hence, the binary EXIT chart is useful for finding the best TH-PPM-UWB-IR-SeCCC system parameter required for attaining a decoding convergence at the lowest possible $\frac{E_b}{N_o}$ value. The best-performing SeCCC schemes shown in Figs. 4 and found from the EXIT chart based design approach are summarised in Table I, which are capable of operating within about 0.9 dB of the AWGN channel's capacity. For the scheme employing $\varphi = 3$, $R_1 = 1/2$ and $R_2 = 3/4$ and characterized in Table I, the distance from capacity is 0.8 dB and 1.8 dB in case of Nakagami-m fading channels. For a bandwidth efficiency of 0.67 bit/s/Hz, the capacity of this scheme [24] is -0.6 dB and 1.0 dB for the quarternary discrete-input AWGN and Nakagami-m fading channels, respectively.

VI. Conclusions

We have designed a near-capacity TH-PPM-UWB-IR-SeCCC system based on EXIT-chart-aided decoding convergence analysis. The system invokes binary RSC codes and different puncturing rates, as summarized in Table I. The puncturer is used to increase the achievable bandwidth efficiency. The interleaver placed before the puncturer helps randomise the puncturing pattern. Optimal SeCCC parameters were found for assisting the TH-PPM-UWB-IR-SeCCC system in attaining decoding convergence at the lowest possible $\frac{E_b}{N_o}$ value, when communicating over uncorrelated Nakagami-m fading channels. The TH-PPM-UWB-IR-SeCCC system designed is capable of operating within about 0.9 dB from the AWGN as well as Nakagami-m fading channel's capacity.

References

[1] Federal Communications Commission, "Revision of part 15 of the commission's rules regarding ultra-wideband transmission systems, first report and order," pp. ET Docket 98–153, 2002.

[2] M. Z. Win and R. A. Scholtz, "Impulse radio: how it works," *IEEE Communications Letters*, vol. 2, pp. 36–38, Feb. 1998.

[3] L.-L. Yang and L. Hanzo, "Residue number system assisted fast frequency-hopped synchronous ultra-wideband spread-spectrum multiple-access: a design alternative to impulse radio," *IEEE Journal on Selected Areas in Communications*, vol. 20, pp. 1652–1663, Dec. 2002.

[4] G. Forney, *Concatenated Codes*. MIT Press, Cambridge, MA,, 1966.

[5] C. Berrou, A. Glavieux, and P. Thitimajshima, "Near Shannon limit error correcting coding and decoding: Turbo codes," *IEEE Transactions on Communications*, pp. 1064–1070, 1993.

[6] C. Shannon, "A mathematical theory of communication," *Bell Syst. Tech. Journal*, vol. 27, pp. 623–656, 1948.

[7] S. Benedetto, D. Divsalar, G. Montorsi, and F. Pollara, "Serial concatenated trellis coded modulation with iterative decoding," in *IEEE International Symposium on Information Theory*, (Ulm), p. 8, June/July 1997.

[8] S. Benedetto, D. Divsalar, G. Montorsi, and F. Pollara, "Self-concatenated trellis coded modulation with self-iterative decoding," in *IEEE Global Telecommunications Conference*, vol. 1, (Sydney, NSW, Australia), pp. 585–591, 1998.

[9] H. A. Loeliger, "New turbo-like codes," in *IEEE International Symposium on Information Theory*, (Ulm), p. 109, June/July 1997.

[10] S. ten Brink, "Convergence behavior of iteratively decoded parallel concatenated codes," *IEEE Transactions on Communications*, vol. 49, pp. 1727–1737, Oct. 2001.

[11] E. Fishler and H. V. Poor, "Low-complexity multiuser detectors for time-hopping impulse-radio systems," *IEEE Transactions on Signal Processing*, vol. 52, pp. 2561–2571, Sept. 2004.

[12] J. Hagenauer, "Rate-compatible punctured convolutional codes (RCPC codes) and their applications," *IEEE Transactions on Communications*, vol. 36, pp. 389–400, Apr. 1988.

[13] S. Benedetto, D. Divsalar, G. Montorsi, and F. Pollara, "A soft-input soft-output APP module for iterative decoding of concatenated codes," *IEEE Communications Letter*, vol. 1, pp. 22–24, January 1997.

[14] M. Z. Win and R. A. Scholtz, "Ultra-wide bandwidth time-hopping spread-spectrum impulse radio forwireless multiple-access communications," *IEEE Transactions on Communications*, vol. 48, pp. 679–689, Apr. 2000.

[15] D. Slepian, "Prolate spheroidal wave functions, Fourier analysis and uncertainty V: The discrete case," *Bell Syst. Tech. Journal*, vol. 57, 1978.

[16] B. Parr, B. Cho, K. Wallace, and Z. Ding, "A novel ultra-wideband pulse design algorithm," *IEEE Communications Letters*, vol. 7, pp. 219–221, May 2003.

[17] H. Sato and T. Ohtsuki, "Frequency domain channel estimation and equalisation for direct sequence ultra wideband (DS-UWB) system," *IEE Proceedings- Communications*, vol. 153, pp. 93–98, Feb. 2006.

[18] A. F. Molisch, "Ultrawideband propagation channels-theory, measurement, and modeling," *IEEE Transactions on Vehicular Technology*, vol. 54, pp. 1528–1545, Sept. 2005.

[19] R. A. Riaz, M. F. U. Butt, S. Chen, and L. Hanzo, "Generic z-domain discrete-time transfer function estimation for ultra-wideband systems," *Electronics Letters*, vol. 44, pp. 1491–1492, Dec. 2008.

[20] M. D. Yacoub, J. E. V. Bautistu, and L. Guerra de Rezende Guedes, "On higher order statistics of the nakagami-m distribution," *IEEE Transactions on Vehicular Technology*, vol. 48, pp. 790–794, May 1999.

[21] L. Hanzo, L.-L. Yang, E.-L. Kuan, and K. Yen, *Single- and Multi-Carrier DS-CDMA: Multi-User Detection, Space-Time Spreading, Synchronisation, Networking and Standards*. New York: John Wiley and Sons, England, 2003.

[22] J. Kliewer, S. X. Ng, and L. Hanzo, "Efficient computation of EXIT functions for nonbinary iterative decoding," *IEEE Transactions on Communications*, vol. 54, pp. 2133–2136, Dec. 2006.

[23] H. Chen and A. Haimovich, "EXIT charts for turbo trellis-coded modulation," *IEEE Communications Letters*, vol. 8, pp. 668–670, Nov. 2004.

[24] L. Hanzo, S. X. Ng, T. Keller, and W. Webb, *Quadrature amplitude modulation: From basics to adaptive trellis-coded, turbo-equalised and space-time coded OFDM, CDMA and MC-CDMA systems*, pp. 746–748. Wiley-IEEE Press, 2nd ed., December 15, 2004.